Human Corneal Endothelial 패턴의 통계적 분석을 위한 광전자적 방법

이 임 걸
한국과학기술연구원, 광전자연구실

Optical–Electronic Method for Statistical Evaluation of Human Corneal Endothelial Patterns

Yim-Kul Lee
Optical Electronics Lab., KIST

Abstract

Hybrid optical-electronic procedures are introduced for the automated estimation of cell parameters (e.g., size, size variation, and shape). Two different optical Fourier analysis procedures are applied to high contrast cell boundary patterns obtained from specular micrographs of the endothelial layer. In one case, a large number of cell patterns are illuminated to extract average cell size information. Once the average cell size information has been obtained, individual cells are illuminated to extract shape infomation.

1. Introdution

The endothelial cell layer consists of some 350,000 to 500,000 polygonal cells. Cells have center–to–center spacings of approximately 20 μm. Their thickness in the longitudinal direction (orthogonal to the plane of observation) is approximately 5 μm. The cells are predominately hexagonal in shape (61~75 %). Cell density decreases with age and disease, as does the degree of hexagonality[1,2]. Under currently–used computer morphometric methods, the polygonal cell boundaries appearing in specular micrographs are traced out by hand or by a computer with strong human intervention. The boundary patterns are then digitized and analyzed by computer. The statistical estimation of morphological parameters is often based on the spatial analysis of only 50 ~ 100 endothelial cells, since the techniques are so slow. This number is often considered too small for clinical evaluation of the corneal tissue, particularly since there might be wide variation in cell size and shape from one region of the cornea to another.

In this paper, an optical-electronic method for the automated evaluation of the endothelial pattern. The method is based on the two dimensional Fourier transform of the cell-boundary pattern[3]. Preliminary results obtained by an optical–digital experiment[4] indicated that the optical Fourier transform obtained from cell boundary patterns could be used to estimate with a good accuracy the average cell density over a wide range (1000 to 3000 $cells/mm^2$); further experiments indicated that shape characteristics could be extracted. One important conclusion of the preliminary experiments was that the optical method could be implemented in such a way that large numbers of cells (> 1000) can be easily be analyzed.

2. Diffraction Pattern Analysis

An input cell boundary pattern is analyzed by a diffraction pattern sampling using a wedge–ring detector (WRD) with 32 wedge detecting elements and 32 semi-annular elements[5-10]. Equations 1 and 2 show a mathematical representation of the data reduction operation in the Fourier transform (FT) plane.

$$R_m = \frac{1}{S_m}\int_{\rho_m}^{\rho_{m+1}}\int_0^{\pi} I(\rho,\varphi)\rho d\rho d\varphi, \quad 1 \le m \le 32 \quad (1)$$

$$A_n = \frac{1}{Q_n}\int_0^{\infty}\int_{\varphi_n}^{\varphi_{n+1}} I(\rho,\varphi)\rho d\rho d\varphi, \quad 1 \le n \le 32 \quad (2)$$

where $I(\rho,\varphi)$ is the Fourier intensity distribution in polar coordinates, and S_m and Q_n are the areas corresponding to the mth ring and nth wedge segments, respectively. The radial projection R_m provides information about the size of the object and is invariant to the orientation of the input object. The angular projection A_n contains shape information on the object and is insensitive to the size of the object. Both R_m and A_n are invariant to horizontal or vertical translation of the object through the invariance of $I(\rho,\varphi)$ to

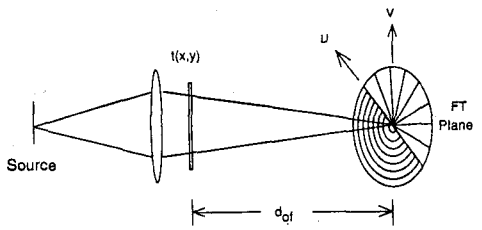

Figure 1. A coherent optical system incorporating a wedge-ring detector (WRD) in the Fourier transform (FT) plane.

such translation. Figure 1 shows a single lens Fourier transforming system with a WRD positioned in the FT plane. With an object $t(x,y)$ illuminated by a converging beam, the output intensity $I(x,y)$ in the FT plane[11] is given by

$$I(x,y) = \frac{A}{\lambda^2 d_{of}^4} \left| T\left(\frac{x}{\lambda d_{of}}, \frac{y}{\lambda d_{of}}\right)\right|^2, \qquad (3)$$

where A is a proportionality factor, λ is the wavelength of the incident quasi-monochromatic light, d_{of} is the distance from the object to the FT plane, and $T(u,v)$ is the FT of $t(x,y)$. In Eq. 3, we assume that the object $t(x,y)$ is fully illuminated (i.e., that the pupil function of the lens can be ignored)[11]. Instead of using a WRD, a CCD camera was used as a detecting device. A WRD with 64 annular rings and 64 wedge sections was simulated on a computer.

Figures 2 and 3 illustrate how the optical diffraction pattern can be used for the statistical estimation of morphological parameters of polygonal cells. Figures 2(a) and (b) show a single hexagon and its optical Fourier intensity pattern. The distance from the origin to the first bright region in the Fourier intensity pattern is inversely proportional to the diameter of the hexagon. Each spoke in the Fourier intensity pattern results from the corresponding parallel sides of the hexagon. The angles (i.e., 60° for a regular hexagon) between two spokes can be used to infer shape characteristics. Figure 2(c) shows the angular projection A_n obtained from the intensity pattern in (b). The locations of the peaks represent the distances in angle of each spoke from a reference angle (e.g., 0°). Figure 3(a) shows an array of regular hexagons and Fig. 3(b) its Fourier intensity pattern. The radial distance from the origin to the first bright region of the FT pattern remains the same as the number of regular hexagons increases. Spoke patterns acquire a spot-like pattern because of sampling effects. The radial projection R_m of the intensity pattern in Fig. 3(b) is shown in Fig. 3(c), the location of the first peak giving information on the size of the hexagon.

As the regularity of the size and orientation in the input pattern is reduced, for example as the regular hexagonal array changes to the corneal pattern array, a speckle-like pattern arises. However, a bright region still forms in the Fourier intensity pattern. Figures 4(a) and (b) show such a cell boundary pattern with random orientation of the cells and variations in size and shape, along with its Fourier intensity pattern. Note in Fig. 4(b) the presence of a central dark ring surrounded by a bright ring. The radial projection of the Fourier intensity pattern is shown in Fig. 4(c). The radius of the first bright ring is estimated by measuring the location of the first peak in the plot of the radial projection. Figure 5 shows the results of locating the peaks for 5 cell patterns with the same cell density ranging from 1000 $cells/cm^2$, but with three sets of different coefficients of average size (CV) variations. It is clear from the high degree of linearity that cell size (or density) can be accurately inferred from measurements of the Fourier intensity patterns. The measurements in Fig. 5 were made by illuminating 100 to 400 cells at a time. By scanning illuminating beam, it is possible to estimate cell density over an entire endothelial pattern, incorporating perhaps several thousand cells in a matter of seconds. That in itself illustrates the power of the hybrid optical method. In addition, a possible measure of the size variation can be made by calculating the contrast or normalized mean-square difference (NMSD) between the first dark and bright regions of the Fourier intensity pattern. Figure 6 shows the NMSD values calculated for 15 patterns, yielding a reasonable good clustering.

It was relatively straightforward to obtain measures of the size and size variation by scanning a number of cells. However, cell shape cannot be determined directly by scanning a large group of cells at a time, since coherent averaging eliminates shape information on individual cells. This coherent averaging effect can easily be seen in Fig. 4 where approximately 200 cells were illuminated. Initial studies[4] indicated that to obtain useful shape information from the FT patterns of cells it is desirable to limit the illuminated area of an input pattern to a small region, i.e., approximately one cell size.

In order to remove the orientational dependence of cells, the angular correlation function, $C(n)$ is cal-

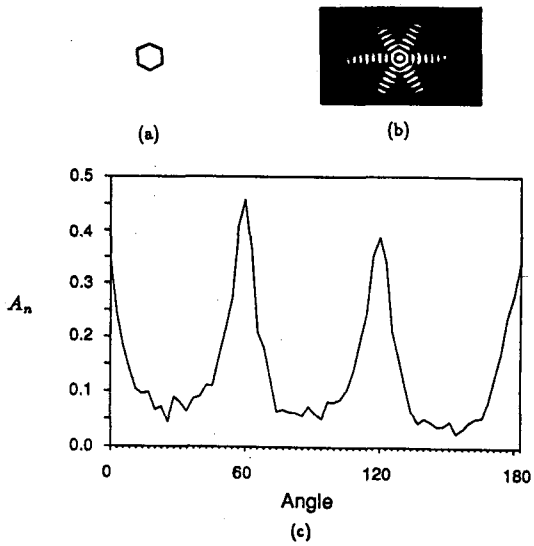

Figure 2. A single hexagonal boundary pattern and its Fourier intensity pattern: (a) boundary pattern; (b) Fourier intensity pattern of (a); (c) angular projection A_n obtained from (b).

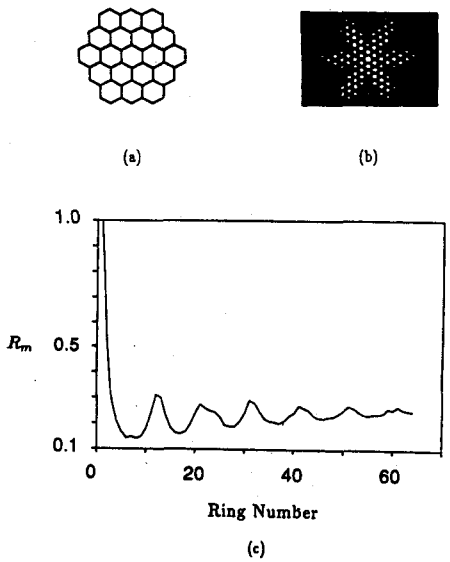

Figure 3. An array of hexagonal boundary patterns: (a) boundary pattern; (b) Fourier intensity pattern of (a); (c) radial projection R_m obtained from (b).

culated from A_n,

$$C(n) = (\sum_{k=1}^{M_W} A_k A_{k+n})/(\sum_{k=1}^{M_W} A_k^2) \quad 0 \le n \le 63 \quad (4)$$

where A_k = the kth component of the angular projection and M_W (= 64) is the number of wedge segments. Figure 7 shows $C(n)$ for the single hexagon of Fig. 2; two well-defined peaks appear at 60° and 120°. The angular correlation function for a regular hexagonal array pattern has similar appearance, though with sampled version.

For an optical experiment for the shape measure, the 24 cells shown in Fig. 8(a) were manually scanned, one cell at a time, with a beam size slightly larger than the fifth cell. Figure 8(b) and (c) show the FT patterns of two cells (Nos. 14 and 15) and their angular correlation functions [= $C(n)$]. The mean $C_m(n)$ of angular correlation functions obtained from 24 numbered cells is shown in Fig. 8(d). $C_m(n)$ in (d) still has well-defined peaks and dips as well as angular lobes, but the peaks are broader with much higher amplitude ratio of dip to peak than those of the hexagonal pattern in Fig. 7. The peaks are located at approximately 60° and 120°. The shape-related characteristics found with individual cell transforms are lost in the Fourier intensity pattern of a large group of cells, as shown in Fig. 4, but preserved, in an average sense, in the mean of the correlation functions associated with these individual cells. It has been observed that the location and width of the peaks in $C_m(n)$ may represent the average shape and the average variation of sides of 24 scanned cells. It is hypothesized that the locations and the widths of the peaks have clinical diagnostic significance in much the same way that percent-of-hexagons and coefficient of average size (CV) do now. For example, pronounced peaks at 60° and 120° on the θ axis suggests a preponderance of hexagonal cells.

3. Concluding Remarks

The experimental results indicate that the Fourier transforms can be analyzed to yield average cell size or density as well as the distribution of sizes. These quantities have major significance in the diagnostic evaluation of the cornea. The diagnostic evaluation of the clinical course of Fuchs' dystrophy can be monitored by an analysis of endothelial morphology. The optical method can also be applied to the morphologic analysis and pattern recognition of retinal photomicrographs. The entire collection of cell patterns, which may number several thousand, can be incorporated in the transform in a fully parallel operation, and thus statistical averaging is done automatically.

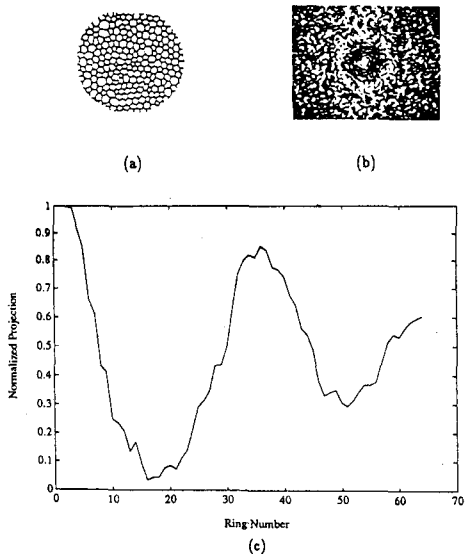

Figure 4. Cell boundary pattern and its Fourier transform: (a) input; (b) Fourier intensity pattern of (a); (c) normalized radial projection of (b).

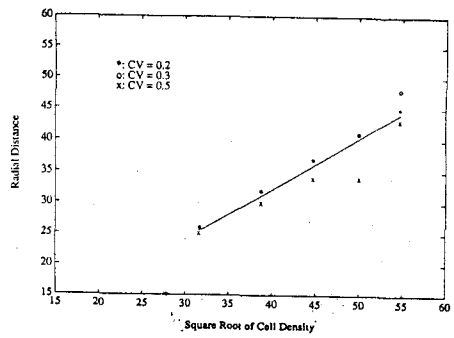

Figure 5. Plot of B_p versus $\sqrt{CD}$ for 15 cell patterns where CD and CD represent the cell density and coefficient of size, respectively. The solid line represents the linear regression of the 15 data points.

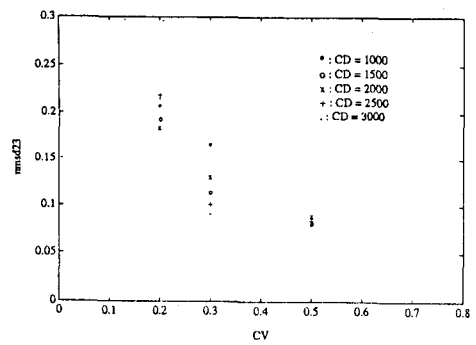

Figure 6. Plot of normalized mean-square difference (NMSD) for 15 cell patterns.

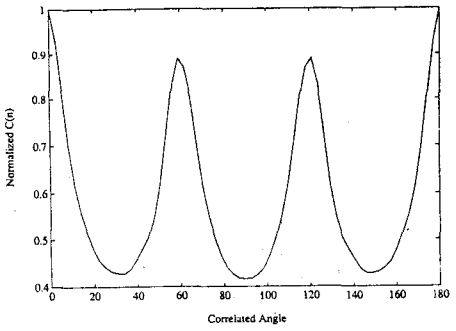

Figure 7. Angular correlation $C(n)$ obtained for the single hexagonal boundary pattern in Fig. 2.

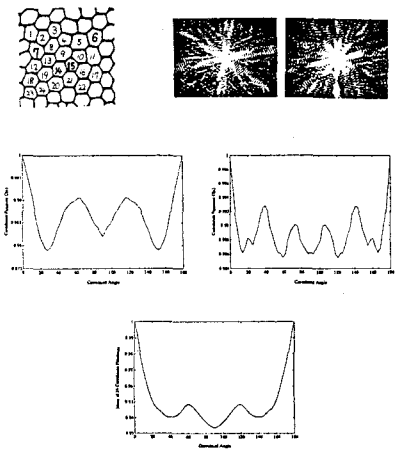

Figure 8. Experimental results using local scans for shape measurement. (a) Upper-left: 24 numbered cells. (b) Upper-right: optical Fourier intensity patterns of cells 14 and 15. (c) Middle: angular correlation functions [= $C(n)$] for cells 14 (left) and 15 (right). (d) Bottom: mean of 26 $C(n)$'s obtained from 24 numbered cells in (a).

References

1. R. W. Yee et. al. "Changes in the normal corneal endothelial cellular pattern as a function of age," *Current Eye Research*, Vol. 4(6), pp. 671–678 (1985).
2. T. Charn-Ling and J. Curmi, "Changes in corneal endothelial morphology in cats as a function of age," *Current Eye Research*, Vol. 7(4), pp. 387-392 (1988).
3. B. R. Masters, "Characterization of corneal specular endothelial photomicrographs by their Fourier transforms," *Proc. SPIE 938*, pp. 246-252 (1988).

4. B. R. Masters, Y. K. Lee, and W. T. Rhodes, "Fourier transform method for statistical evaluation of corneal endothelial morphology," in *Noninvasive Diagnostic Techniques in Ophthalmology*, (B. R. Masters, ed.), pp. 122-141, New York, NY:Springer-Verlag (1990).

5. G. G. Lendaris and G. L. Stanley, "Diffraction-pattern sampling for automatic pattern recognition," in *Proc. IEEE*, pp. 198–216 (1970).

6. H. L. Kasdan, "Industrial applications of diffraction pattern sampling," *Optical Engineering*, Vol. 18(5), pp. 496-503 (1979).

7. B. Pernick et. al., "Screening of cervical cytological samples using coherent optical processing," *Applied Optics*, Vol. 17(1), pp. 21-33 (1978).

8. C. Gorecki, "Optical/digital analyzer of Fe_2O_3 substrate by Fourier techniques," *Optical Engineering*, Vol. 27(6), pp. 466-470 (1988).

9. D. P. Casasent et. al., "Diffraction pattern sampling using a computer–generated hologram," *Applied Optics*, Vol. 25(6), pp. 983–989 (1986).

10. M. J. Simpson, "Diffraction pattern sampling using a holographic optical element in an imaging configuration," *Applied Optics*, Vol. 26(9), pp. 1786–1791 (1987).

11. J. Goodman, *Introduction to Fourier Optics*, New York, NY: McGraw–Hill (1968).

12. L. W. Hirst, K. Yamauchi, C. Enger, W. Vogelpohl, and V. Whittington, "Quantitative analysis of wide-field specular microscopy," *Invest. Ophth. Vis. Sci*, Vol. 30, , pp. 1972–1979 (1989).